Eur. Phys. J. D **44**, 371–379 (2007)
DOI: 10.1140/epjd/e2007-00188-3

THE EUROPEAN PHYSICAL JOURNAL D

Spectroscopic studies of laser induced aluminum plasma using fundamental, second and third harmonics of a Nd:YAG laser

N.M. Shaikh, S. Hafeez, B. Rashid, and M.A. Baig[a]

Atomic and Molecular Physics Laboratory, Department of Physics, Quaid-i-Azam University, 45320 Islamabad, Pakistan

Received 16 February 2007 / Received in final form 30 April 2007
Published online 13 June 2007 –

Abstract. In the present work, we have studied the spatial evolution of the aluminum plasma produced by the fundamental (1064 nm), second (532 nm) and third (355 nm) harmonics of a Q-switched pulsed Nd:YAG laser. The experimentally observed line profiles of neutral aluminum have been used to extract the excitation temperature using Boltzmann plot method whereas the electron number density has been determined from the Stark broadened profiles. Besides we have studied the variation of excitation temperature and electron number density as a function of laser irradiance at atmospheric pressure. In addition, we have performed quantitative analysis of photon absorption and vapor ionization mechanism at three laser wavelengths and estimated the inverse bremsstrahlung (IB) absorption and photoionization (PI) coefficients. The validity of the assumption of local thermodynamic equilibrium is discussed in the light of the experimental results.

PACS. 32.30.Jc Visible and ultraviolet spectra – 32.70.Jz Line shapes, widths, and shifts – 32.80.-t Photon interactions with atoms

1 Introduction

Pulsed laser ablation has raised tremendous interest in the last few years, as demonstrated by the large number of experimental and theoretical studies conducted on the subject. It provides a powerful and flexible tool in a wide class of research applications spanning from material science to the field of medicine. For example, thin films of almost all materials grown by pulsed laser deposition (PLD) possess unique properties. At the same time, many studies highlighted various physical processes involved in the phenomenon as well as of in situ monitoring of the process itself. This is accomplished by using the experimental techniques typically employed in atomic, molecular and plasma physics [1]. In the laser-induced breakdown spectroscopy an intense laser beam is focused on the surface of a target which generates a micro plasma. This technique is divided in to three regions, (i) interaction of the laser beam with the target material resulting in the evaporation of the surface layers; (ii) interaction of the evaporated material with the incident laser beam resulting in an isothermal plasma formation and expansion; and (iii) anisotropic adiabatic expansion of the ablated vapor cloud in vacuum (or into a back ground gas). The first two regimes start with the emergence of the laser pulse and continue until the duration of the laser pulse, whereas the last regime starts after the termination of the laser pulse [2].

The laser induced plasma characteristics depend on several parameters including the features of the target, properties of the ambient medium, laser wavelength and pulse duration etc. Cabalin and Laserna [3] studied the effect of laser wavelength on the ablation threshold for metals with different thermal properties (from Zn to W) using the first (1064 nm), second (532 nm) and forth (266 nm) harmonics of a Nd:YAG laser. The fluence threshold was shown to be the lowest for the longest wavelengths (1064 nm), whereas the energy threshold was the lowest for the shortest wavelength (266 nm). There are numerous experimental studies devoted to the effect of laser parameters on the evaporation process, plume and plasma characteristics, and analytical performance of LIBS. Russo and co-workers [4–6] investigated the effect of laser irradiance on electron density and plume temperature, for a Nd:YAG laser at 266 nm on glass or silicon samples. The effect of laser pulse duration on the laser induced plasma emission, electron density and plume temperature has also been reported [7–9]. Different researchers have studied the induced plasma on different target materials like carbon, lead, lithium, sodium and copper using different laser sources. Sabsabi and Cielo [10] used the fundamental mode of a Nd:YAG laser to study the plasma produced at the surface of aluminum in air at atmospheric pressure. Lu et al. [11] studied the aluminum plasma generated by an excimer laser (248 nm) in vacuum using an optical multichannel analyzer. Colon et al. [12] measured

[a] e-mail: baig@qau.edu.pk

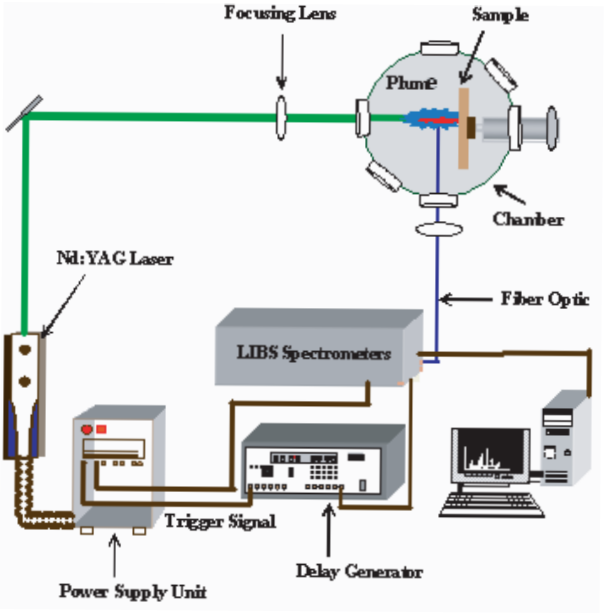

Fig. 1. (Color online) Schematic diagram of the experimental set-up.

the Stark broadening parameters of some of the Al II transition lines in the atmosphere of molecular nitrogen.

In the present work, we have studied the effect of the laser wavelength and fluence on the emission lines and also on the plasma parameters of aluminum. A Q-Switched Nd:YAG laser operating at its fundamental (1064 nm), second (532 nm) and third (355 nm) harmonic has been used to ablate the aluminum surface. Excitation temperatures and electron number density have been calculated at different positions along the direction of propagation of the plasma. In addition we have discussed the laser absorption via inverse bremsstrahlung (IB) and photoionization (PI) processes for these three laser wavelengths. The effect of the self-absorption and the minimum criteria for the local thermodynamic equilibrium (LTE) is also discussed.

2 Experimental details

A schematic diagram of the experimental set-up shown in Figure 1 is similar as in our previous work [13–15]. The energy source used in the experiments was a Q-switched Nd:YAG (Quantel Brilliant) laser, pulse duration of 5 ns and 10 Hz repetition rate. The laser beam was focused through a 20 cm quartz lens on the sample in a chamber. The sample was mounted on a 3-dimensional sample stage, which was rotated to provide a fresh surface after each laser pulse to avoid deep crater. The distance between the focusing lens and the sample was less than the focal length of the lens to prevent any breakdown of the ambient gas in front of the target. The emission from the plume was registered by the LIBS2000 (Ocean optics Inc.) detection system in conjunction with an optical fiber (high-OH, core diameter: 600 μm) having a collimating lens (0–45° field of view), placed at right angle to the direction of the plasma expansion. The optical emission of the plasma was observed through a 5 cm diameter fused silica window. The emission signal was corrected by subtracting the dark signal of the detector through the LIBS software. The LIBS2000 detection system is equipped with five spectrometers each having 5 μm slit width, covering the range between 200–720 nm. Each spectrometer has 2048 element linear CCD array and an optical resolution of ≈0.06 nm. The LIBS2000 detection system and the Q-switch of the Nd:YAG laser were synchronized. The LIBS2000 system triggered the Q-switch of the Nd:YAG laser and the flash lamp out of the Nd:YAG laser triggered the LIBS2000 detection system through a four-channel digital delay/pulse generator (SRS DG 535). The out put data were averaged for 10 laser shots. The system has been calibrated in wavelength by recording the well-known lines of neon, argon and mercury covering the wavelength range 200–720 nm. The uncertainties in the measurement are ≈0.02 nm. All the five spectrometers installed in the LIBS2000 are manufacturer calibrated in efficiency using the DH-2000-CAL standard light source. The data acquired simultaneously by all the five spectrometers were stored on a PC through the OOI LIBS software for subsequent analysis.

3 Results and discussion

In the first set of experiments the 1064 nm laser has been used to ablate the material. The spectrum of the Al plasma was recorded at different positions along the direction of the propagation of the plasma. The spectrum reveals a number of neutral as well as ionic lines of aluminum. The neutral aluminum lines at 226.90 nm correspond to $5d\ ^2D_{5/2} \rightarrow 3p\ ^2P_{3/2}$ transition, 336.70 nm, 337.31 nm to $4d\ ^2D_{3/2,5/2} \rightarrow 3p\ ^2P_{1/2,3/2}$, transitions, 308.21 nm, 309.28 nm to $3d\ ^2D_{3/2,5/2} \rightarrow 3p\ ^2P_{1/2,3/2}$ transitions, 394.40 nm, 396.15 nm to $4s\ ^2S_{1/2} \rightarrow 3p\ ^2P_{1/2,3/2}$ transitions and 669.60 nm to $5p\ ^2P_{3/2} \rightarrow 4s\ ^2S_{1/2}$ transition. The lines at 281.61 nm ($4s\ ^2S_0 \rightarrow 3p\ ^2P_1$) 358.65 nm ($4f\ ^3F_3 \rightarrow 3d\ ^3D_3$) and 466.30 ($4p\ ^1P_1 \rightarrow 3P^2\ ^1D_2$) belong to signally ionized aluminum, whereas the observed transition lines belonging to doubly ionized aluminum are 360.19 nm ($3d\ ^2D_{3/2} \rightarrow 4p\ ^2P_{3/2}$), 361.23 nm ($3d\ ^2D_{3/2} \rightarrow 4p\ ^2P_{1/2}$), 370.20 nm ($4p\ ^2P_{1/2} \rightarrow 5s\ ^2S_{1/2}$) and 371.31 nm ($4p\ ^2P_{3/2} \rightarrow 5s\ ^2S_{1/2}$) shown in Figures 2a and 2b. Some impurity lines due to magnesium Mg II, at 279.55 nm, Mg I, at 279.83 nm and 285.21 nm have also been detected. The assignment of these lines is done using the NBS (NIST) database. Similarly the spatial distribution of the transition lines has been recorded using the 532 nm and 355 nm lasers. In all the three laser wavelengths the fluence is kept at $\approx 5.5 \times 10^{10}$ W cm^{-2}.

3.1 Excitation temperature and electron number density

The excitation characteristics of the laser produced plasma are determined from the plasma properties such

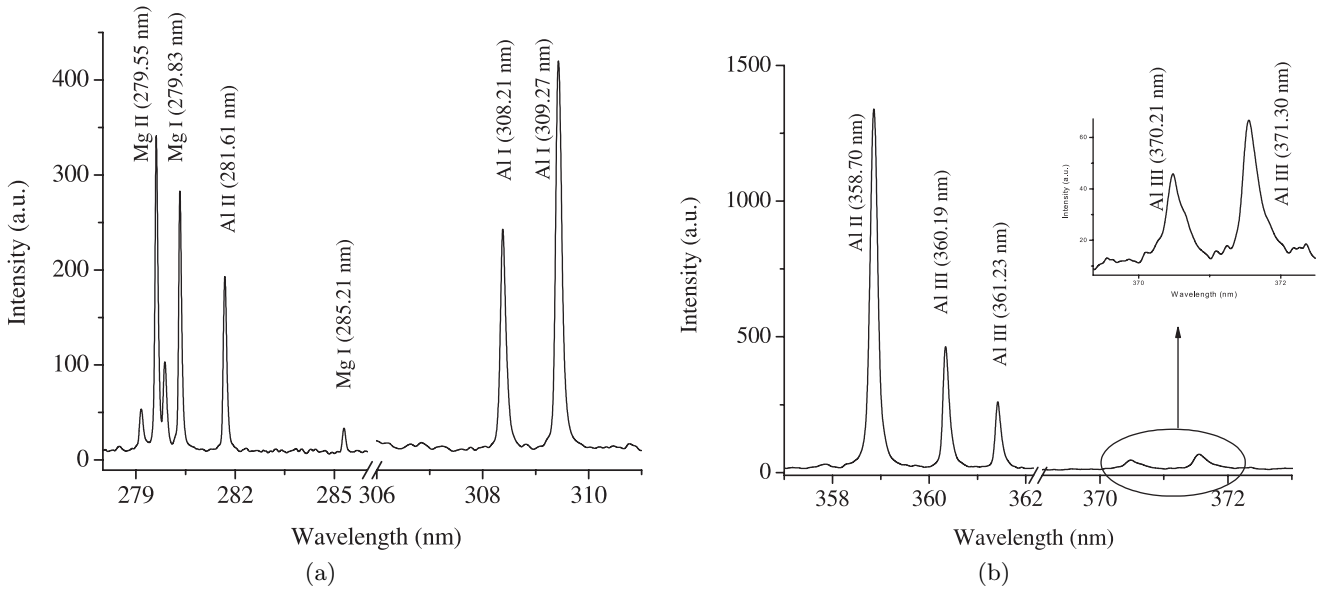

Fig. 2. The emission spectrum generated by the 1064 nm laser showing predominately the spectral lines originating from transitions in the neutral and singly ionized and doubly aluminum and magnesium.

Table 1. Spectroscopic parameters of neutral Al transition lines.

Wavelength λ (nm)	Transitions	Statistical weight g_k	g_i	Transition probability A (s^{-1})	Upper level energy E_k (cm^{-1})
257.51	$4d\ ^2D_{5/2} \rightarrow 3p\ ^2P_{3/2}$	6	4	2.8×10^7	38 933.97
265.24	$5s\ ^2S_{1/2} \rightarrow 3p\ ^2P_{1/2}$	2	2	1.3×10^7	37 689.41
308.21	$3d\ ^2D_{3/2} \rightarrow 3p\ ^2P_{1/2}$	4	2	6.3×10^7	32 435.45
309.28	$3d\ ^2D_{3/2} \rightarrow 3p\ ^2P_{3/2}$	4	4	7.4×10^7	32 436.79
394.40	$4s\ ^2S_{1/2} \rightarrow 3p\ ^2P_{3/2}$	2	4	4.9×10^7	25 347.75
396.15	$4s\ ^2S_{1/2} \rightarrow 3p^2P_{1/2}$	2	2	9.8×10^7	25 347.75

as temperature and electron number density. The analytical measurements are generally performed after the initial plasma, when a state of local thermal equilibrium (LTE) sets in. The population of the excited states follows the Boltzmann distribution and their relative emissivity (I_{mn}) is given as [16,17],

$$\ln\left(\frac{\lambda_{mn} I_{mn}}{g_m A_{mn}}\right) = \ln\left(\frac{N(T)}{U(T)}\right) - \frac{E_m}{kT_{exc}}, \qquad (1)$$

where λ_{mn}, A_{mn} and g_m is the wavelength, the transition probability and the statistical weight of the upper level, respectively. E_m is the excited level energy, T_{exc} is the excitation temperature, k is the Boltzmann constant, $U(T)$ is the partition function and $N(T)$ is the total number density of atoms. From equation (1), a plot of $\ln(\lambda_{mn} I_{mn}/g_m A_{mn})$ versus E_m for the observed spectral lines follow a straight line and its slope $-1/kT_{exc}$ yields the excitation temperature. The transition lines at 265.24 nm, 257.51 nm, 308.21 nm, 309.27 nm, 394.40 nm and 396.15 nm have been used to draw the Boltzmann plot. The relevant spectroscopic parameters for these transitions, taken from NIST database, are listed in Table 1.

In LIBS, two spectroscopic methods are commonly used to determine the electron number density. The first method requires measure of the Stark broadening of the spectral lines and the second method requires the measure of the population ratio of two successive ionization states of the same element. The emission spectral lines of the laser produced plasma are noticeably broadened therefore electron number density can be extracted from the widths of the spectral lines. There are two important line broadening mechanisms in the laser plasma i.e. Doppler broadening and Stark broadening. The Doppler broadening can be estimated from the relation [18,19]

$$\Delta\lambda = 2\lambda\sqrt{\frac{2kT\ln 2}{mc^2}}, \qquad (2)$$

here λ (m) is the wavelength, k ($J\,K^{-1}$) is the Boltzmann constant, T (K) is the absolute temperature, m (kg) is the atomic mass and c ($m\,s^{-1}$) is the velocity of light. At a temperature of 10 000 K, the Doppler width is estimated $\approx$0.005 nm for the transition at 396.15 nm. This width is too small to be detected in the present studies, therefore it is neglected. The Stark broadening of the spectral lines in the neutral and singly ionized species occur when an emitting atom at a distance r from an ion or electron is perturbed by the electric field. The FWHM of the Stark broadened profile is related with the number density

through the relation [20–23]

$$\Delta\lambda_{1/2} = 2\omega\left(\frac{N_e}{10^{16}}\right) + 3.5A\left(\frac{N_e}{10^{16}}\right)^{1/4} \times \left[1 - \frac{3}{4}N_D^{-1/3}\right]\omega\left(\frac{N_e}{10^{16}}\right), \quad (3)$$

here $\Delta\lambda_{1/2}$ is the width of the spectral line, ω is the electron impact broadening parameter, A is the ion impact broadening parameter, N_e is the electron number density and N_D is the number of particles in the Debye sphere. This relation consists of two terms; the first term is the contribution of electron impact broadening in the line width and the second term represents the contribution of ion impact broadening. The line width is predominantly associated with the first term only as the effect of the ion impact broadening parameter is relatively very small. Therefore, the second term can safely be ignored and the relation governing the width of a spectral line may be written in a much simpler form as:

$$\Delta\lambda_{1/2} = 2\omega\left(\frac{N_e}{10^{16}}\right). \quad (4)$$

The true line width $\Delta\lambda_{1/2}$ is determined by subtracting the instrumental line width from the experimentally observed line profile [4]. The instrumental width of the LIBS 2000 spectrometer system is extracted as 0.05(2) nm using a narrow line width dye laser. The value of ω has been taken from reference [24]. The extracted electron number density contains about 15% error attributed to uncertainties in the width measurement, the instrumental width de-convolution and the electron impact parameter.

The condition that the atomic and ionic states should be populated and depopulated predominantly by electron collisions, rather than by radiation, requires an electron density which is sufficient to ensure the high collision rate. The corresponding lower limit of the electron density is given by McWhirter criterion [25]:

$$N_e \geqslant 1.6 \times 10^{12} T^{1/2} \Delta E^3, \quad (5)$$

where T (K) is the plasma temperature and ΔE (eV) is the energy difference between the states, which are expected to be in local thermodynamic equilibrium (LTE). At a temperature ~10 000 K, equation (5) yields $N_e \approx 10^{15}$ cm^{-3}, which ascribe the validity of LTE. The use of the emission spectroscopy for the measurement of temperature and electron number density requires optically thin spectral lines. The aluminum plasma is observed to be optically thin as in case of self absorption the strong lines appear to have either a flat toped profile (saturation) or a dip at the central frequency (self absorption) [26]. The self absorption depends on the oscillator strength, level energies degeneracy, broadening parameters and also on the plasma parameters [17]. In the present work we did not find any saturation or dip at the central frequency of the observed emission lines.

In the spatial behavior of the plasma generated by the 1064 nm, 532 nm, and 355 nm lasers, at irradiance of

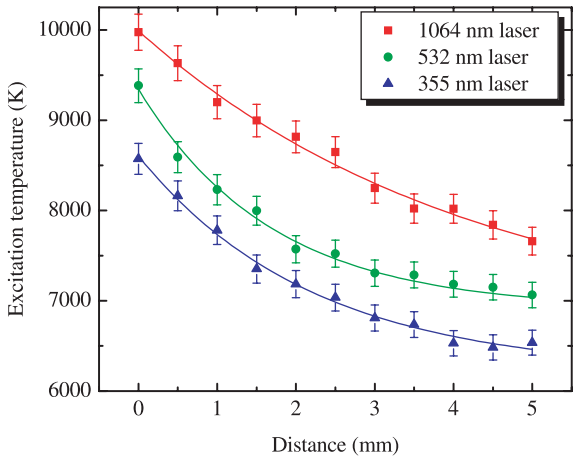

Fig. 3. (Color online) Variation of the excitation temperature along the direction of propagation of the plume using 1064 nm, 532 nm and 355 nm lasers.

≈5.5×10^{10} W cm^{-2}. The excitation temperature close to the surface of the target is estimated as 9630 K, 8590 K and 8160 K respectively. This temperature decreases to 7660 K, 7065 K and 6525 K at about 5 mm from the target as shown in Figure 3. The number density close to the target in the case of 1064 nm, 532 nm and 355 nm lasers are 1.3×10^{18} cm^{-3}, 1.7×10^{18} cm^{-3} and 2.7×10^{18} cm^{-3}, these values decreases to 4.2×10^{17} cm^{-3}, 5.1×10^{17} cm^{-3} and 9.3×10^{17} cm^{-3} at about 5 mm from the target respectively, shown in Figure 4. The plasma temperature decreases steeply as a function of distance from the target. A high value of the temperature at the surface of the target is attributed to the absorption of the laser energy via the inverse bremsstrahlung (IB) process. The IB process is usually described by the inverse absorption length (α_{ib}), which is given by [27–30]:

$$\alpha_{ib}(\text{cm}^{-1}) \approx 1.37 \times 10^{-35} \lambda^3 N_e^2 T_e^{-1/2}. \quad (6)$$

Here λ (μm) is the wavelength of the laser photons, T_e (K) is the electron temperature, and N_e (cm^{-3}) is the electron density. In the case of fundamental 1064 nm laser, the IB absorption α_{ib} is approximately equal to 0.29 cm^{-1} at the laser irradiance of 5.5×10^{10} W cm^{-2}. This implies that 1.6×10^8 W cm^{-2} is absorbed in the plasma plume, which is nearly four times greater than the 532 nm laser and six times greater than 355 nm laser. It is evident from Figure 3 that the temperature is greater in the case of 1064 nm laser than 532 nm and 355 nm lasers. Thus the IB process is more efficient in the case of IR as compared to 532 nm and 355 nm lasers because of its λ^3 dependence (see Fig. 3). The decrease of the excitation temperature away from the target is attributed to the fact that thermal energy is rapidly converted into the kinetic energy of the plasma, which causes expansion of the plasma. Different values of number densities for three different laser wavelengths depend upon the coupling of the laser light with the target. The reflection of the light from the metal also plays an important role which depends on the thermal conductivity, roughness and laser wavelength. In the

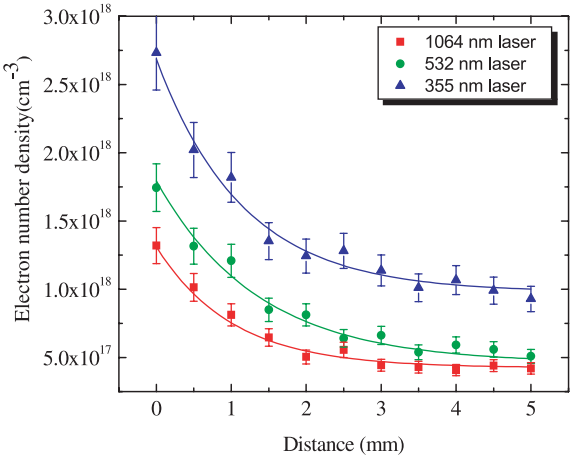

Fig. 4. (Color online) Variation of the electron number density along the direction of propagation of the plume using 1064 nm, 532 nm and 355 nm lasers.

case of aluminum metal the reflectivity for the 1064 nm, 532 nm and 355 nm lasers are ≈0.95, 0.92 and 0.92 respectively [31]. The infrared laser has a relatively higher reflectivity as compared to the visible and ultraviolet (UV) radiation. Once the plasma is formed, its growth is governed by the photoionization (PI) and multiphoton ionization (MPI) process of the excited atoms. The first excited state of aluminum lies 3.14 eV above the ground state, whereas the ionization potential is 5.99 eV. Thus with the UV photons (3.46 eV at 355 nm) the PI process of the excited states is more probable, whereas in the visible (2.31 eV at 532 nm) and IR (1.17 eV at 1064 nm) two-photon ionization and three-photon ionization is required. Thus the number density in the case of 355 nm laser is higher than that of 532 nm and 1064 nm lasers. As it is clear from Figure 4, the number density has the highest value for 355 nm laser, which can be attributed to the fact that the mass ablation is higher for 355 nm and has minimum value for the 1064 nm laser.

In the case of UV laser, direct photoionization (PI) of the excited atoms becomes the dominant ionization mechanism. The photoionization process is given by [1,29,30]

$$\alpha_{PI} = \sigma_{PI} N_n \approx \sum_n 2.9 \times 10^{-17} \frac{(E_n)^{5/2}}{(h\nu)^3} N_n, \qquad (7)$$

where σ_{PI} is the photoionization cross-section, $h\nu$ (eV) is the photon energy, E_n (eV) is the ionization energy and N_n (cm^{-3}) is the number density of the excited state n. In this equation the summation is performed over the energy levels which satisfy the condition $h\nu > E_n$. Note that the above equation, although derived for hydrogen like atoms, can be applied to complex atomic systems as discussed by Amoruso et al. [28]; and Zel'dovich and Raizer [29]. The electrons generated by the photoionization process are not in thermal equilibrium and the recombination process reduces the number density of the electrons and ions generated by photoionization. The decrease of N_e is mainly due to the recombination between the electrons and ions in the plasma. On the other hand, the recombination process can counterbalance the electron generation by electron impact (EI) ionization and photo ionization (PI). If the recombination time constant is comparable to the laser pulse duration, an electron generated by the ionization process can effectively contribute to the IB absorption. The rate of recombination can be estimated by considering the relaxation time of the three-body recombination and photo-recombination process. In particular the rate of the EI from the first aluminum excited state ($\varepsilon = 3.14$ eV) τ_{EI}^{-1} is given as [28,29]

$$\tau_{EI}^{-1} \approx 2 \times 10^{-10} N^* \left(\frac{I_{\rm H}}{I_{\rm Al} - \varepsilon^*} \right)^2 T_e^{0.5} \exp\left(-\frac{I_{\rm Al} - \varepsilon^*}{T} \right), \qquad (8)$$

where, N^* is the excited state number density, and $I_{\rm H}$ (13.6 eV) and $I_{\rm Al}$ (5.99 eV) are the hydrogen and aluminum ionization potentials respectively. An appropropriate estimate of N^* can be obtained from the Boltzmann equilibrium condition, at $T_e \sim 1$ eV: we obtained EI ionization time constant $\tau_{EI} < 1$ ns. This is clearly sufficient for the enhancement of the ionization during the laser pulse duration (∼5 ns). Therefore, the vapors reach quite readily the degree of ionization at which the IB by electron-ion (e-i) collision becomes the primary mechanism of photon absorption, and a highly absorbing plasma is produced.

The effectiveness of PI of the excited atoms in a nanosecond pulse UV and visible laser ablation of metallic targets have been demonstrated by Chang and Warner [30]; Song and Xu [32]; Lunney and Jordan [33]. A similar effect of laser wavelengths was reported by Fabbro et al. [34] who used a Nd: glass laser at fundamental, second and forth harmonics at 1.06 μm, 0.53 μm and 0.26 μm, respectively. Dittrich and Wennrich [35] discussed the effect of laser wavelength and inferred that the mass ablation rate increases with the shorter wavelength. Abdellatif and Imam [36] reported the effect of laser wavelength on the temperature and electron number density of the aluminum plasma produced by the fundamental, SHG and THG of the Nd:YAG laser. Barthe'lemy et al. [37] also studied the effect of laser wavelength on the axial and temporal behavior of temperature and electron number density of the aluminum plasma, ablated by the 1064 nm, 532 nm and 266 nm of a Nd:YAG laser with 6 ns pulse duration.

In the second set of the experiment we have investigated the effect of the laser irradiance on the emission intensity, width and shift of the transition lines as well as on the plasma parameters. We have observed that the intensities and the widths of the spectral lines increase with an increase in the laser irradiance. In the case of 1064 nm laser the irradiance was increased from 1.3×10^{10} to 4.3×10^{10} W cm^{-2} and a shift in the neutral aluminum transition lines at 256.79 nm, 257.51 nm, 265.24 nm, 266.04 nm, 308.21 nm, 309.27 nm, 394.40 nm, and 396.15 nm have been observed as 0.03 nm, 0.02 nm, 0.017 nm, 0.02 nm 0.04 nm, 0.03 nm, 0.01 nm and 0.01 nm respectively. The observed shifts and widths of these lines are shown in Figure 5. At a lower fluence the vapour produced by the leading edge of the laser pulse

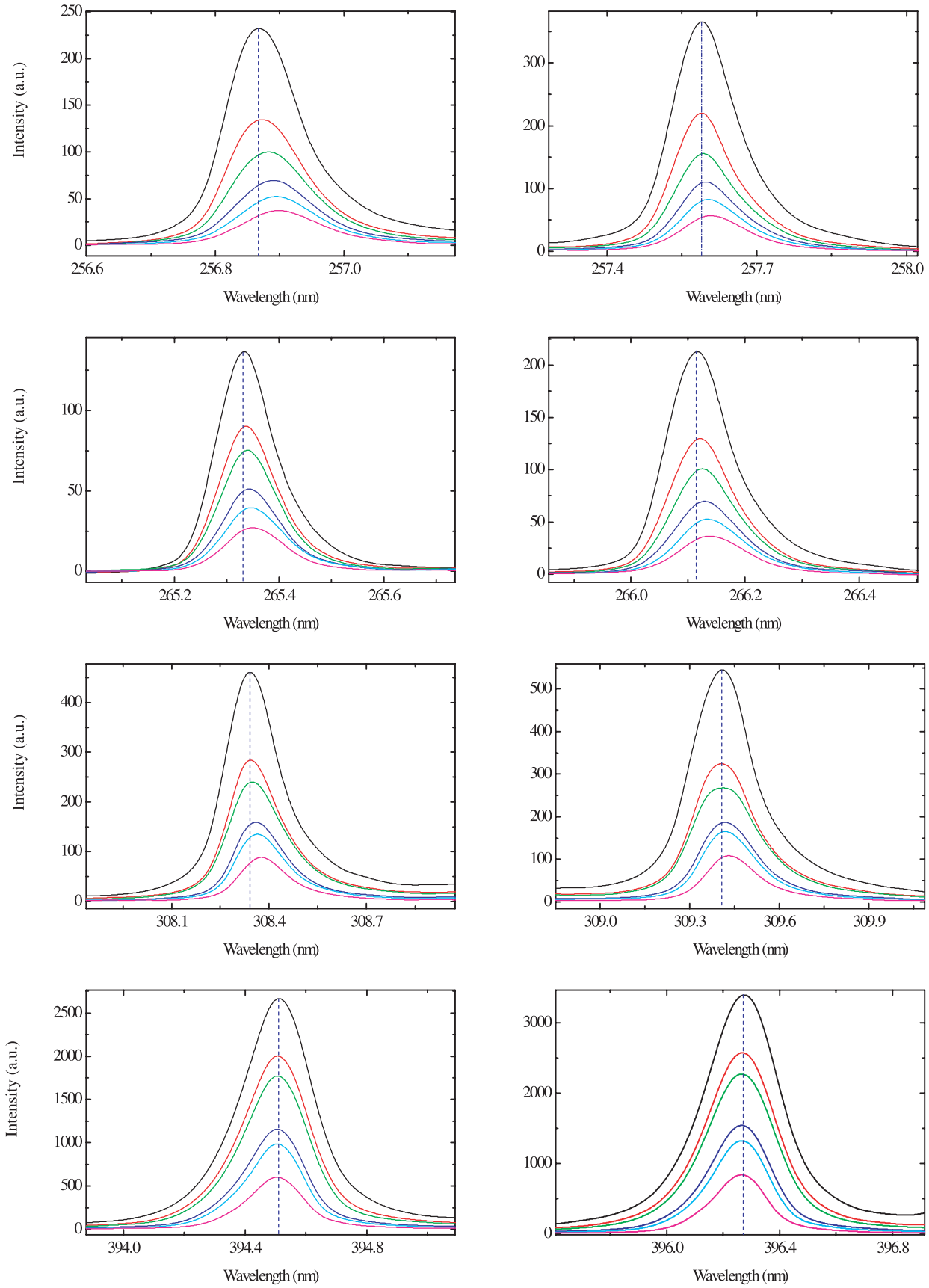

Fig. 5. (Color online) Variation in the signal intensity and width of the Al (I) lines at 256.79 nm, 257.51 nm, 265.24 nm, 266.04 nm, 308.21 nm, 309.27 nm, 394.40 nm, and 396.15 nm at different values of 1064 nm laser.

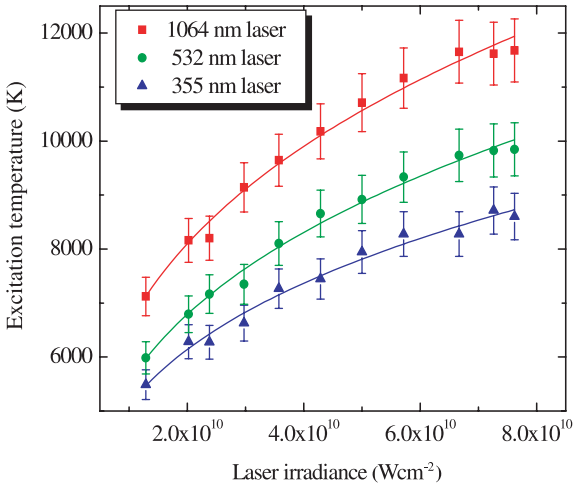

Fig. 6. (Color online) Variation of the excitation temperature with the laser irradiance using 1064 nm, 532 nm and 355 nm lasers.

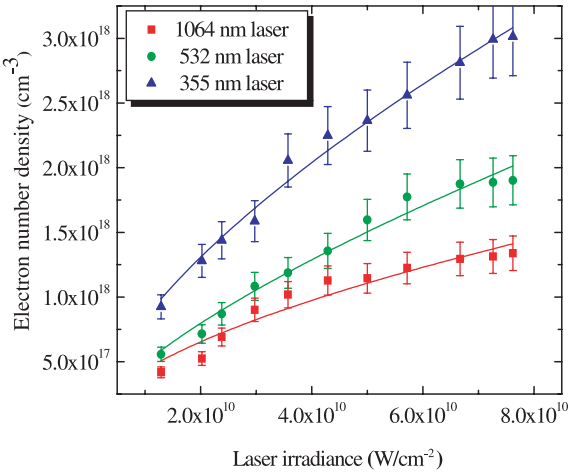

Fig. 7. (Color online) Variation of the electron number density with the laser irradiance using, 1064 nm, 532 nm and 355 nm lasers.

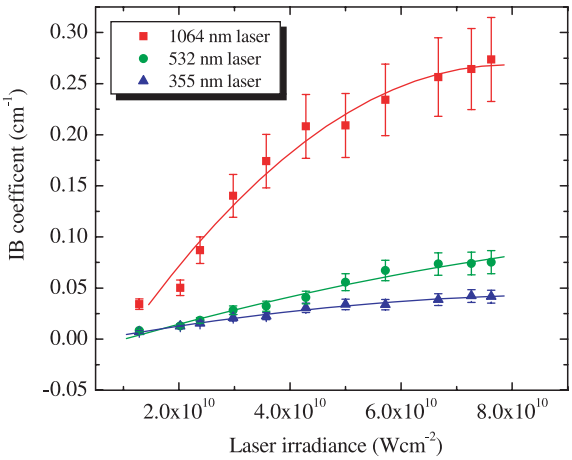

Fig. 8. (Color online) Variation of the calculated inverse bremsstrahlung absorption α_{IB} with the laser irradiance at 1064 nm, 532 nm and 355 nm lasers.

behaves like a thin medium, so the laser passes nearly unattenuated through the vapour. However with an increase in the laser fluence the rate of evaporation as well as the laser absorption (IB and PI processes) in the plasma increases, which causes an increase in intensity and width of the spectral lines. At a higher irradiance above the 6.0×10^{10} W cm^{-2}, the variation is very small due to plasma shielding. Plasma shielding effects in the laser-ablation processes at high power density have also been reported by several authors [38–41].

We have determined the excitation temperature and electron number density as a function of laser irradiance in three modes of a Nd:YAG laser. The laser irradiance ranges from 1.3×10^{10} to 7.6×10^{10} W cm^{-2}, the excitation temperature varies as (7 120 to 11 680) K, (5 985 to 9 850) K and (5 490 to 8 600) K, whereas the number density varies as $(4.2 \times 10^{17}$ to $7.6 \times 10^{18})$ cm^{-3}, $(5.6 \times 10^{17}$ to $1.9 \times 10^{18})$ cm^{-3} and $(9.2 \times 10^{17}$ to $3.3 \times 10^{18})$ cm^{-3} for the 1064 nm, 532 nm and 355 nm lasers respectively. The temperature and number density as a function of laser irradiance are fitted to a power law. In the case of fundamental (1064 nm; $T \sim I^{0.29\pm0.01}$, and $N_e \sim I^{0.57\pm0.02}$), SHG (532 nm; $T \sim I^{0.28\pm0.01}$, and $N_e \sim I^{0.64\pm0.03}$) and THG (355 nm; $T \sim I^{0.26\pm0.01}$, and $N_e \sim I^{0.70\pm0.02}$), shown in Figures 6 and 7 respectively. At the initial stage of the plasma near the ablated surface, there are a large number of electrons, ions and the atoms in the excited state, therefore at the surface the plasma progressively behaves like an optically thick medium and effectively shields the target surface from the tailing part of the laser pulse. At $\lambda = 532$ nm, the ionization can mainly be ascribed to electron neutral inverse bremsstrahlung (IB) processes and consequently electron ionization, whereas for the 355 nm laser, direct photoionization of the excited states in the vapor seems to be the most effective process. The IB process is less effective in the UV than in the visible and IR. The longer wavelength corresponds to a lower photon energy and lower probability of photoionization from the excited levels, resulting in a lower absorption coefficient. Figures 8–10 depicts the calculated IB coefficient, PI coefficient and the percentage absorption via PI process in the plasma, as a function of laser irradiance for the three laser wavelengths. It is clear from the Figures 8 and 9 that the plasma absorption via IB process is dominating for the longer wavelength, whereas the PI process is dominating for the shorter wavelength. At 1064 nm laser, the amount of plasma absorption is much lower than that of 532 nm and 355 nm lasers, in spite of the fact that the IB absorption coefficient is significantly higher. This is attributed to much lower number densities of electrons, ions and neutrals in the plasma. Figure 10 shows that the plasma absorption in both the processes increases with the laser irradiance. The amount of laser energy effectively penetrating the sample can be approximated as [42]:

$$E \sim I_0(1 - R)(1 - A)$$

where I_0, R and A stands for the incident laser irradiance, the target reflectivity and the percentage absorption in

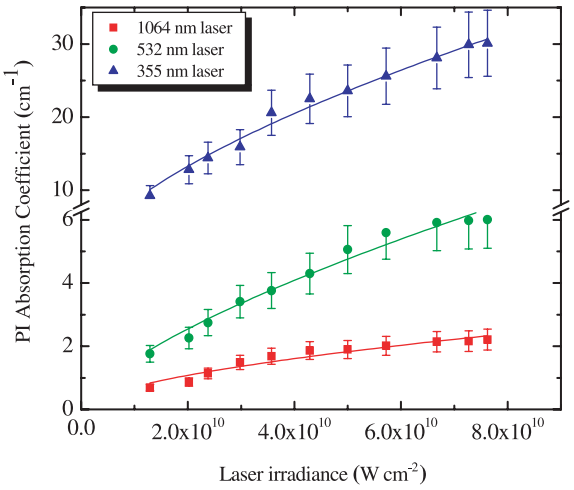

Fig. 9. (Color online) Variation of the calculated photoionization absorption α_{PI} with the laser irradiance at 1064 nm, 532 nm and 355 nm lasers.

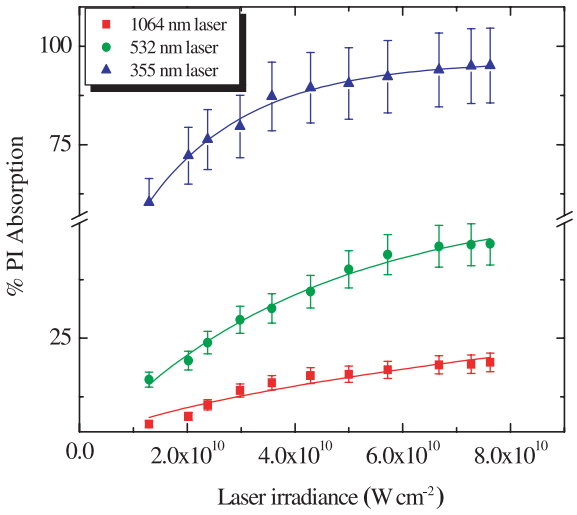

Fig. 10. (Color online) Calculated percentage amount of laser absorption via PI absorption with the laser irradiance at 1064 nm, 532 nm and 355 nm lasers.

the plasma, respectively. At the three laser wavelengths, fundamental, SHG and THG having laser irradiance of $\sim 1.3 \times 10^{10}$ W cm^{-2}, it yields:

- at 1064 nm: $E \sim 1.3 \times 10^{10}\ (1 - 0.06)(1 - 0.95) = 6.0 \times 10^{8}$ W cm^{-2};
- at 532 nm: $E \sim 1.3 \times 10^{10}\ (1 - 0.16)(1 - 0.92) = 8.6 \times 10^{8}$ W cm^{-2};
- at 355 nm: $E \sim 1.3 \times 10^{10}\ (1 - 0.6)(1 - 0.92) = 4.1 \times 10^{8}$ W cm^{-2}.

Whereas at a higher irradiance, 7.6×10^{10} W cm^{-2}, these values become 3.0×10^{9} W cm^{-2}, 3.3×10^{9} W cm^{-2} and 3.0×10^{8} W cm^{-2} respectively. These calculated results show that in the case of 1064 nm and 532 nm lasers the plasma absorption as well as penetration into the sample increases with the laser irradiance, but different behavior has been observed for the 355 nm laser, in which the plasma absorption increases and the laser penetration into the sample decreases with the increase of the laser irradiance.

Conclusion

A space-resolved diagnostic technique has been used to study the emission from the plume of aluminum (Al) plasma produced by the fundamental second and third harmonics of a Nd:YAG laser. The observed intensities of the atomic and ionic transition lines in the case of 355 nm laser is the strongest as compared to the 532 nm, and 1064 nm lasers, due to maximum coupling of the UV laser with the sample target. The excitation temperature and the number density are found to be higher close to the target and decrease exponentially away from the target. The temperature for the 1064 nm laser is higher than that for the 532 nm and 355 nm lasers at the same value of laser irradiance. It is because of the inverse bremsstrahlung process, which is dominant for the longer wavelength lasers, whereas the number density for the 355 nm laser is higher than that of the 532 nm and 1064 nm lasers, because of the competing effects of the target surface reflectivity and the laser plasma absorption.

We have also studied the behavior of the plasma at different laser irradiance and it is observed that not only the intensity and width of the atomic and ionic transition lines increases with the increase of the laser irradiance but also the transition lines are found to be slightly shifted. The plasma parameters such as temperature and number density are found to increase with the laser irradiance. It is inferred that at first stage the laser vapor interaction is largely due to the inverse bremsstrahlung (IB) process, which is dominant in the case of 1064 nm laser. However, in the UV and visible lasers, photoionization of the excited species plays a dominant role. Both the mechanisms efficiently increase the electron density, and probably trigger the breakdown ionization during the laser pulse duration. It is remarked that the target heating, melting, vaporization, ionization degree and densities of the ions and electrons in the plume and also the plasma shielding all increase with the laser irradiance.

We are grateful to the Quaid-i-Azam University, Islamabad and Higher Education Commission (HEC), for providing necessary funds to acquire the LIBS equipment. Nek Muhammad, Babar Rashid and Sarwat Hafeez are grateful to HEC for providing the scholarships for the Ph.D. research work.

References

1. S. Amoruso, R. Bruzzese, N. Spinelli, R. Velotta, J. Phys. B: At. Mol. Opt. Phys. **32**, R131 (1999)
2. R.K. Singh, J. Narayan, Phys. Rev. B **41**, 8843 (1990)
3. L.M. Cabalin, J.J. Laserna, Spectrochim. Acta B **53**, 723 (1998)
4. S.S. Mao, X. Zeng, X. Mao, R.E. Russo, J. Anal. At. Spectrom. **19**, 495 (2004)

5. H.C. Liu, X.L. Mao, J.H. Yoo, R.E. Russo, Spectrochim. Acta B **54**, 1607 (1999)
6. H.C. Liu, X.L. Mao, J.H. Yoo, R.E. Russo, Appl. Phys. Lett. **75**, 1216 (1999)
7. G.W. Rieger, M. Taschuk, Y.Y. Tsui, R. Fedosejevs, Spectrochim. Acta B **58**, 497 (2003)
8. H. Borchert, K. Darée, M. Hugenschmidt, J. Phys. D: Appl. Phys. **38**, 300 (2005)
9. B. Le Drogoff, J. Margot, F. Vidal, S. Laville, M. Chaker, M. Sabsabi, T.W. Johnston, O. Barthélemy, Plasma Sources Sci. Technol. **13**, 223 (2004)
10. M. Sabsabi, P. Cielo, Appl. Spectrosc. **49**, 499 (1995)
11. Y. Lu, Z.Tao, M. Hong, Jpn J. Appl. Phys. **38**, 2958 (1999)
12. C. Colon, G. Hatern, E. Verdugo, P. Ruiz, J. Campos, J. Appl. Phys. **73**, 4752 (1993)
13. N.M. Shaikh, S. Hafeez, B. Rashid, S. Mahmood, M.A. Baig, J. Phys. D: Appl. Phys. **39**, 4377 (2006)
14. N.M. Shaikh, B. Rashid, S. Hafeez, Y. Jamil, M.A. Baig, J. Phys. D: Appl. Phys. **39**, 1384 (2006)
15. N.M. Shaikh, B. Rashid, S. Hafeez, S. Mahmood, M. Saleem, M.A. Baig, J. Appl. Phys. **100**, 073102 (2006)
16. V. Detalle, R. Héon, M. Sabsabi, L. St-Onge, Spectrochim. Acta B **56**, 1011 (2001)
17. B. Le Drogoff, J. Margot, M. Chaker, M. Sabsabi, O. Barthélemy, T.W. Johnston, S. Laville, F. Vidal, Y. von Kaenel, Spectrochim. Acta B **56**, 987 (2001)
18. A.P. Thorne, *Spectrophysics 2* (Chapman and Hall, London, 1988), p. 169
19. G.V. Marr, *Plasma Spectroscopy* (Elsevier publishing company, 1968)
20. G. Bekefi, C. Deutsch, B. Yaakobi, *Principles of Laser Plasmas*, edited by G. Bekefi (Wiley, New York, 1976), p. 549
21. C. Colon, A. Alonso-Medina, C. Herran-Martinez, J. Phys. B: At. Mol. Opt. Phys. **32**, 3887 (1999)
22. A.H. El-Astal, T. Morrow, J. Appl. Phys. **80**, 1156 (1996)
23. H.C. Liu, X.L. Mao, J.H. Yoo, R.E. Russo, Spectrochim. Acta B **54**, 1607 (1999)
24. H.R. Griem, *Plasma Spectroscopy* (McGraw-Hill Inc., 1964)
25. R.W.P. McWhirter, *Plasma Diagnostic Techniques*, edited by R.H. Huddlestone, S.L. Leonard (Academic, New York, 1965), Chap. 5
26. D.A. Cremers, L.J. Radzimski, *Hand book of Laser-induced Breakdown Spectroscopy* (John Wiley & Sons Ltd, 2006)
27. C. Colon, A. Alonso-Medina, Spectrochim. Acta B **61**, 856 (2006)
28. S. Amoruso, M. Armenante, V. Berardi, R. Bruzzese, N. Spinelli, Appl. Phys. A **65**, 265, (1997)
29. Ya.B. Zel'dovich, Yu.P. Raizer, *Physics of Shock Waves and High Temperature Hydrodynamic Phenomena* (Academic, New York, 1967)
30. J.J. Chang, B.E. Warner, Appl. Phys. Lett. **69**, 473 (1996)
31. *Hand book of Chemistry and Physics*, edited by D.R. Lide, H.P.R. Frederikse, 84th edn. (CRC Press, Boca Raton, FL, 2003–2004)
32. K.H. Song, X. Xu, Appl. Phys. A **65**, 477 (1997)
33. J.G. Lunney, R. Jordan, Appl. Surf. Sci. **127–129**, 941 (1998)
34. R. Fabbro, E. Fabre, F. Amiranoff, C. Garban-Labaune, J. Virmont, M. Weinfeld, C.E. Max, Phys. Rev. A **26**, 2289 (1980)
35. K. Dittrich, R. Wennrich, Prog. Anal. At. Spectrosc. **7**, 139 (1984)
36. G. Abdellatif, H. Imam, Spectrochim. Acta B **57**, 1155 (2002)
37. O. Barthe'lemy, J. Margot, M. Chaker, M. Sabsabi, F. Vidal, T.W. Johnston, S. Laville, B. Le Drogoff, Spectrochim. Acta B **60**, 905 (2005)
38. B. Wollf-Rottke, J. Ihlemann, H. Schmidt, A. Scholl, Appl. Phys. A **60**, 13 (1995)
39. V.N. Tokarev, J.G. Lunney, W. Marine, M. Sentis, J. Appl. Phys. **78**, 1241 (1995)
40. R. Jordan, J.G. Lunney, Appl. Surf. Sci. **127–129**, 215 (1998)
41. H. Schittenelm, G. Callies, P. Berger, H. Hugel, J. Phys. D: Appl. Phys. **29**, 1564 (1996)
42. A. Bogaerts, Z. Chen, Spectrochim. Acta B **60**, 1280 (2005)